Pramana – J. Phys. (2017) 88:90
DOI 10.1007/s12043-017-1410-3

Thermal decay rate of a metastable state with two degrees of freedom: Dynamical modelling versus approximate analytical formula

I I GONTCHAR[1,2] and M V CHUSHNYAKOVA[2,3,*]

[1]Physics and Chemistry Department, Omsk State Transport University, Omsk, Russia
[2]Physics Department, Omsk State Technical University, Omsk, Russia
[3]Institute of Physics and Technology, Tomsk Polytechnic University, Tomsk, Russia
*Corresponding author. E-mail: maria.chushnyakova@gmail.com

MS received 9 June 2016; revised 11 December 2016; accepted 25 January 2017; published online 1 June 2017

Abstract. Accuracy of the Kramers approximate formula for the thermal decay rate of the metastable state is studied for the two-dimensional potential pocket. This is done by comparing with the quasistationary rate resulting from the dynamical modelling. It is shown that the Kramers rate is in agreement with the quasistationary rate within the statistical errors provided the absorptive border is far enough from the potential ridge restricting the metastable state. As the absorptive border (or its part) gets closer to the ridge, the Kramers formula underestimates the quasistationary rate. The difference reaches approximately the factor of 2 when the absorptive border coincides with the ridge.

Keywords. Metastable system; quasistationary decay rate; Kramers rate; dynamical modelling.

PACS Nos 24.60.–Ky; 05.60.–k; 82.20.–Pm

1. Introduction

One encounters the problem of thermal decay of a metastable (quasistationary) state in many branches of physics, chemistry and biology: fission of excited nuclei and dissociation of a molecule are just two examples (see e.g. refs [1–10]).

The rate of thermal decay of a metastable (quasistationary) state in the presence of friction is evaluated for one-dimensional motion using the formulas derived by Kramers in ref. [11] or their modifications [12–15]. The rates calculated according to those formulas are expected to agree with the long time limit of the escape rate obtained using either the stochastic differential equations (the Langevin equations) or the corresponding partial differential equations (the Fokker–Planck equation or the Smoluchowski equation). The rate is referred to as the quasistationary dynamical rate (QDR) and denoted as R_{D} henceforth.

The problem of agreement between the approximate analytical rates (Kramers rates, R_{K}) and R_{D} (which is supposed to be exact within the statistical and numerical errors) was studied in several works [13–18] for the case of one degree of freedom (1D). In particular, in [13–16] the applicability of the Kramers formula for the case of high temperature was studied. In [12,15] corrections to the Kramers formula were proposed which account for the anharmonicity of the potential. In [13,14] the concept of the mean first passage time (developed long time ago in [19,20]) was applied for the microcanonical ensemble. In [14], for the first time by our knowledge, the dependence of the QDR on the position of the absorptive border was studied for the harmonic potential (i.e. the potential constructed of two smoothly joined parabolas). It was shown in that work that when the absorptive border is far away from the barrier point, the Kramers formula agrees with the QDR, whereas as the border gets closer to the barrier the QDR exceeds the Kramers rate significantly (see figures 1 and 2 in ref. [14]). In ref. [13], from the concept of the mean first passage time, a correction to the Kramers formula was obtained that accounts for the final distance between the barrier and absorptive points (see eq. (23) in that work). This correction goes over to factor 2 when these two points coincide. Let us note that the consideration in refs [13–18] was restricted to the case of the overdamped motion.

In refs [21–23] the Kramers formula was generalized for the case of several degrees of freedom. Every now

and again these generalizations were confronted with results of numerical modelling [23–25]. However, to our knowledge, a systematic comparison for the multidimensional problem is absent in the literature. In particular, it is not studied whether the influence of the absorptive border in the 2D case is the same, as for the 1D case. The aim of the present work is to remedy the situation to a certain extent.

In his pioneering work [11], Kramers indicated the atomic nuclear fission process as one of the three physical problems for which his results might be applied. Presently vast literature exists on the application of the Kramers approach to nuclear fission (see e.g. refs [3,4,13,21,23–30]). Our work stems from the nuclear fission problem too. Therefore, we devote special attention to the cases with typical dependences of the potential upon the collective coordinates. We also take into account the 'distance' between the position of the potential barrier and the absorptive border. However, the results obtained might be of general interest as many features of the model (e.g. the canonical ensemble, the coordinate-independent friction and inertia parameters, the single-barrier potential) are common in different applications of the Brownian motion.

The paper is organized as follows. Section 2 is devoted to the description of the model. Approximate analytical formula as well as the recipe for calculating the quasistationary dynamical decay rate are discussed here. In §3, we compare the Kramers rate with the QDR for different potential landscapes and different lay-outs of the absorptive border. The friction strength is also varied. In §4, we summarize our results. In Appendix A, we discuss the details of finding the QDR and its errors. In Appendix B, the table comprising the parameters of the modelling is presented.

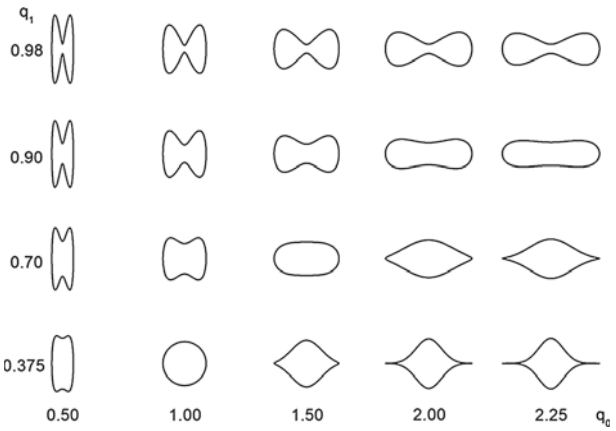

Figure 1. The shapes of the fissioning nucleus for different values of deformation parameters (only mirror-symmetric fission is considered).

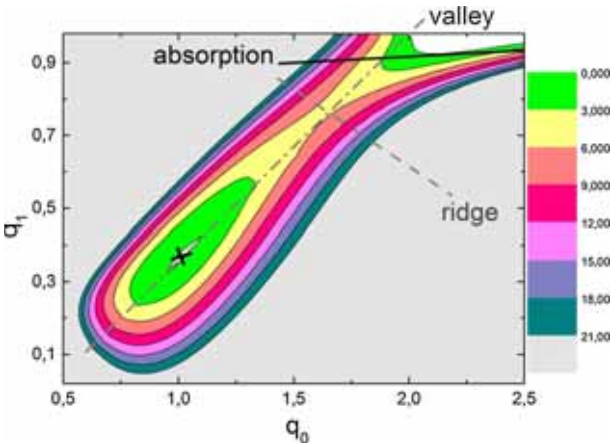

Figure 2. The realistic potential energy landscape for ^{218}Ra along which the Brownian particle (fissioning nucleus) moves. The energy is calculated within the framework of the LSD model [31]. The ground state (cross), the ridge, the fission valley as well as the typical absorptive (scission) line are also shown.

2. The model

2.1 *The scenario*

The motion of the Brownian particle is characterized by two collective coordinates q_0 and q_1 which we consider to be dimensionless. In the case of nuclear fission, q_0 is responsible for the elongation of the fissioning nucleus and q_1 represents the necking of the shape. Figure 1 illustrates the relation between the coordinates and the shape (only mirror-symmetric fission is considered). Note that the odd shapes like in the upper left and lower right corners of this figure possess extremely large potential energies and therefore are never reached during the modelling. Figure 2 represents the potential landscape along which the Brownian particle moves. This is a realistic potential energy corresponding to the symmetric fission of ^{218}Ra calculated within the framework of the Lublin–Strasbourg drop (LSD) model [31]. This figure reflects typical mutual lay-out of the ground state, the ridge, and the fission valley. For the present work, this figure is of illustrative character.

In the LSD model [31], the Coulomb, surface, and curvature terms are deformation-dependent and significant for the Brownian particle motion. In order to calculate the potential energy within the framework of this model, we developed our own computer code and compared the results with the potential energy surfaces represented in [9]. Since for the dynamical calculations a model potential (see eqs (1)–(7) below) is used in the present work, we omit the discussion of details of the LSD potential.

At the initial moment of time, the particle is located near the metastable state with the coordinates $q_{0c} = 1.00, q_{1c} = 0.375$ (see figures 1, 2). In the case of nuclear fission, this corresponds to the situation when the nucleus has spherical shape. Because of thermal fluctuations, the Brownian particle can reach the barrier point with the coordinates q_{0b}, q_{1b} or its vicinity, i.e. the ridge separating the quasistationary state from the valley in the upper-right corner of figure 2. The difference between the potential energies at q_{0c}, q_{1c} and q_{0b}, q_{1b}, $U_b - U_c$, is called the barrier height in nuclear fission or the activation energy in chemical reactions. Henceforth we set $U_c = 0$. After reaching the ridge, the particle can return to the quasistationary state due to fluctuations or move further to the absorptive border due to the driving force. The absorptive border in nuclear fission corresponds to the scission line at which the nucleus separates quickly into two fragments.

In the present work, for the potential energy we use the following analytical ansatz:

$$U(q_0, q_1) = U_{P2}(q_0) + C_1(q_1 - q_{1\mathrm{v}})^2/2, \tag{1}$$

$$U_{P2}(q_0) = \begin{cases} C_0(q_0 - q_{0c})^2/2 & \text{at } q_0 < q_{0m}; \\ U_b - C_0(q_0 - q_{0b})^2/2 & \text{at } q_0 > q_{0m}. \end{cases} \tag{2}$$

Here

$$q_{1\mathrm{v}}(q_0) = q_{1c} + \frac{q_{1b} - q_{1c}}{q_{0b} - q_{0c}}(q_0 - q_{0c}), \tag{3}$$

$$q_{0m} = (q_{0b} + q_{0c})/2, \tag{4}$$

$$C_0 = U_b/(q_{0b} - q_{0c})^2. \tag{5}$$

Equations (4) and (5) guarantee smooth connection of two pieces of the potential in eq. (2) at $q_0 = q_{0m}$. The stiffness C_1 is taken to be q_0-dependent. We approximate this dependence using the formula [24]

$$C_1 = C_{1\mathrm{as}}\left\{1 + w\left[1 + \exp\left(\frac{2q_0 - q_{0c} - q_{0b}}{q_{0c} - q_{0b}}\right)\right]^{-1}\right\}. \tag{6}$$

Here $C_{1\mathrm{as}}$ is the asymptotic value of the stiffness ($C_1 => C_{1\mathrm{as}}$ as $q_0 => \infty$) and w controls the evolution of the width of the valley from the ground state to the saddle state and beyond.

We presume that the absorptive border (subscript a) is represented by a straight line whose equation reads as

$$q_{1a} = q_{1s} + k_0(q_0 - q_{0s}). \tag{7}$$

Two examples of the potential energy maps for ^{218}Ra used for the dynamical modelling are presented in figure 3. They are calculated using eqs (1)–(5). As in figure 2, the ridge, the fission valley, and the typical absorptive (scission) lines are also shown. Figure 3a corresponds to the case of $q_{1b} = q_{1c}$ which is referred to as 'perpendicular valley'. The cases $q_{1b} \neq q_{1c}$ will be referred to as 'diagonal valley'. One such case with $q_{1b} = 2q_{1c}$ is presented in figure 3b. One sees that the analytical potential presented in figure 3b reproduces the distinct features of the realistic potential shown in figure 2.

The angles ϕ_{1r} and ϕ_{ra} shown in the figure are defined as follows. The angle of rotation of the ridge relative to the q_1-axis is denoted as ϕ_{1r} whereas the angle of rotation of the absorptive border relative to the ridge is denoted as ϕ_{ra} (the angles are positive in the case of the anticlockwise rotation). The coefficient k_0 in eq. (7) is

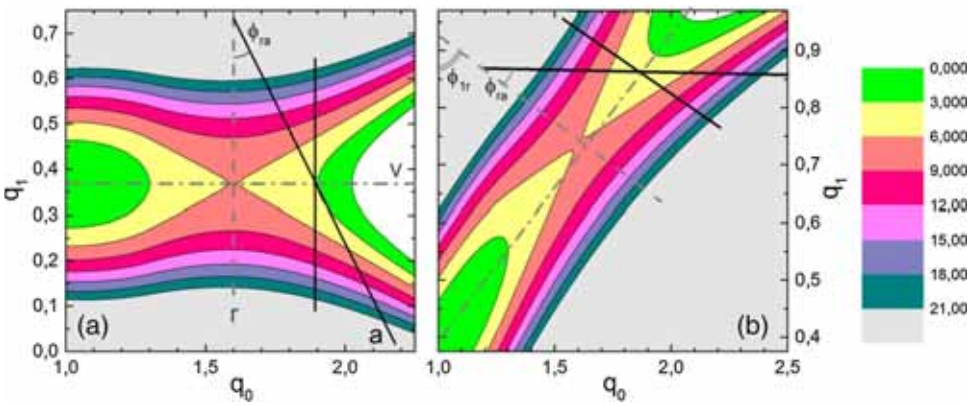

Figure 3. Two analytical potential energy landscapes calculated using eqs (1)–(5) for ^{218}Ra. As in figure 2 the ridge (r), the fission valley (v), and the typical absorptive (scission) lines (a) are also shown. (**a**) corresponds to $q_{1b} = q_{1c}$ ('perpendicular valley') and (**b**) corresponds to $q_{1b} \neq q_{1c}$ ('diagonal valley').

related to these angles in the following way:

$$k_0 = -1/\tan(\phi_{ra} + \phi_{1r}). \tag{8}$$

The perpendicular valley in figure 3a corresponds to $\phi_{1r} = 0$; in figure 3b, $\phi_{1r} = 0.56$ (note that the vertical and horizontal scales are different in the figures).

2.2 *Dynamical equations and the corresponding decay rates*

The time evolution of the dynamical variables of the Brownian particle is described by the stochastic differential equations (the Langevin equations). For the two-dimensional case, these equations read (see, e.g. [3]) as

$$\frac{\mathrm{d}p_i}{\mathrm{d}t} = -(\partial_i \mu_{jk}) p_j p_k/2 - \eta_{ij}\mu_{jk}p_k + K_i + g_{ij}\Gamma_j, \tag{9}$$

$$\frac{\mathrm{d}q_i}{\mathrm{d}t} = \mu_{ik}p_k. \tag{10}$$

The symbol ∂_i denotes the partial derivative with respect to q_i. The time evolution of the system is defined by the inverse inertia tensor μ_{jk}, the friction tensor η_{ij}, the driving forces $K_i = -\partial_i U$, the random forces $g_{ij}\Gamma_j$. Equations (9) and (10) represent a generalization of the classical dynamical Hamilton equations when the mechanical system moves under the influence of dissipative forces and fluctuations.

The amplitudes of the random forces are related to the temperature and the components of the friction tensor by the fluctuation–dissipation theorem:

$$g_{ik}g_{kj} = T\eta_{ij}. \tag{11}$$

In nuclear physics, the temperature T is measured in MeV as the potential energy, thus the Boltzmann constant is equal to 1. The random values Γ_i are taken to represent white noise

$$\langle \Gamma_i \rangle = 0, \tag{12}$$

$$\langle \Gamma_i(t_1)\,\Gamma_j(t_2)\rangle = 2\delta_{ij}\delta(t_1 - t_2)\,. \tag{13}$$

In the discrete form corresponding to the Euler–Maruyama method [32], the Langevin equations read as

$$p_i^{(n+1)} = p_i^{(n)} + \Delta p_i, \tag{14}$$

$$q_i^{(n+1)} = q_i^{(n)} + \Delta q_i, \tag{15}$$

$$\Delta p_i = -\{(\partial_i \mu_{jk}) p_j p_k/2 + \eta_{ij}\mu_{jk}p_k - K_i\}\tau + g_{ij}b_j\sqrt{\tau}, \tag{16}$$

$$\Delta q_i = \mu_{ik}^{(n)}(p_k^{(n)} + p_k^{(n+1)})/2. \tag{17}$$

The superscripts represent two moments of time separated by the interval τ, which is equal to the time step of numerical modelling. In the rhs of eq. (16) all quantities correspond to the time moment $n\tau$. The random numbers b_j entering the random forces have a Gaussian distribution with zero averages and variances equal to 2.

Although in the fission problem the inertia and friction tensors are deformation-dependent, in this work we ignore this dependence and consider the tensors to be diagonal:

$$\eta_{ij} = k_\eta \eta \delta_{ij} = k_\eta \hbar (n_0 A)^{4/3} r_0^4 \delta_{ij}, \tag{18}$$

$$\mu_{ij} = \frac{\delta_{ij}}{m} = \left(r_0^2 m_0 A^{5/3}\right)^{-1}\delta_{ij}. \tag{19}$$

Here $n_0 = 0.17\,\mathrm{fm}^{-3}$ is the nucleon saturation density, $r_0 = 1.22\,\mathrm{fm}$, $m_0 = 0.01044\,\mathrm{MeV}\cdot\mathrm{zs}^2/\mathrm{fm}^2$ is the nucleon mass, the dimensionless parameter k_η allows to vary the friction strength, m is the mass of the Brownian particle.

The definition of the time-dependent decay rate reads as

$$R_{\mathrm{at}}(t) = -\frac{1}{\Pi(t)}\frac{\mathrm{d}\Pi}{\mathrm{d}t}. \tag{20}$$

Here $\Pi(t)$ is the probability that the metastable state has not yet decayed by the time moment t.

Equations (14)–(17) describe the Markovian process, i.e. the memory effects are not taken into account. The equations are solved numerically using random numbers. The solution is actually a sequence of N_{tot} trajectories, all terminated not later than at the moment of time t_{D}. Some of those trajectories reach the absorptive border before t_{D}. The decay rate is calculated in this algorithm as follows:

$$R_{\mathrm{at}} = \frac{1}{N_{\mathrm{tot}} - N_{\mathrm{at}}}\frac{\Delta N_{\mathrm{at}}}{\Delta t}. \tag{21}$$

Here N_{at} is the number of Brownian particles (or stochastic trajectories) which have reached the absorptive border by the time moment t and ΔN_{at} is the number of particles which have reached the absorptive border during the time interval Δt. In order to find R_{D} we choose several bins beginning from the end of R_{at}-array (i.e. from the time moment t_{D}) and average R_{at} over these bins. This procedure and its errors are discussed in detail in ref. [33] (see also Appendix A).

Typical behaviour of R_{at} is shown in figure 4. Here and below, for all the figures involving the decay rate, the parameters of the calculations are collected in table B1. After a transient stage, the decay rate reaches its quasistationary value R_{D}. Each time we checked whether the results of modelling did not depend upon the time step within the statistical errors. The value of τ typically

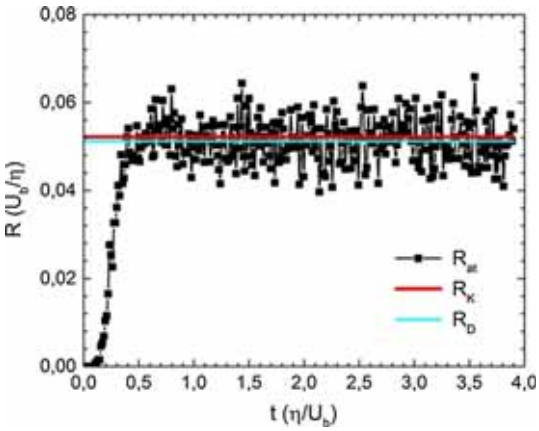

Figure 4. The typical time dependence of the dynamical decay rate $R_{\rm at}$ (oscillating line with boxes). The horizontal lines indicate the QDR ($R_{\rm D}$) and the Kramers rate ($R_{\rm K}$, see eq. (22)). See parameters of the calculations in table B1.

was varied from 0.05 up to 0.20 zs. In order to calculate the quasistationary decay rate with relative error 1% or smaller, about 10,000 fissioned trajectories were obtained.

Although the transient stage does not influence the value of $R_{\rm D}$ which is the focus of the present work, its dependence on the barrier height and temperature might be interesting by itself. For the 1D case, this problem was considered in [34,35]. For the multidimensional case this dependence should be considered in a separate study, in particular because it takes much larger statistics (number of dynamical trajectories) than for calculating $R_{\rm D}$.

2.3 *Approximate analytical decay rate*

The generalization of the Kramers formula obtained in refs [21,22] reads as

$$R_{\rm K} = \omega_{\rm K} \left\{ \frac{|\det U_c''|\, \det m_b}{|\det U_b''|\, \det m_c} \right\}^{1/2} \exp(-U_b/T). \qquad (22)$$

Here $\det U_c''$ ($\det U_b''$) is the determinant of the second derivatives of the potential energy at the quasistationary (saddle) point; $\det m_c$ ($\det m_b$) is the determinant of the inertia tensor at the quasistationary (saddle) point. The multiplier $\omega_{\rm K}$ is the only positive root of the equation

$$\det \left\{ m_{ij}\omega_{\rm K}^2 + \eta_{ij}\omega_{\rm K} - \frac{\partial^2 U}{\partial q_i \partial q_j} \right\}_b = 0. \qquad (23)$$

Equation (22) is supposed to be valid if:

(i) the potential barrier is high enough compared to the temperature;
(ii) the absorptive border is far enough from the barrier (ridge);
(iii) the quasistationary point is far enough from the barrier (ridge);
(iv) the potential is represented well by the portions of parabolas near the quasistationary and saddle states.

3. Results

3.1 *Absorptive border far from the ridge*

Let us first study how the Kramers rate measures up against QDR when the absorptive border is far enough from the ridge. The simplest case is when the valley goes along the q_0 coordinate (perpendicular valley). Then the only thing which can matter is the dependence of C_1 in eq. (1) upon q_0. Figure 5 illustrates this evolution for several values of w (see eq. (6)). The increase of C_1 with q_0 (when $w < 0$) should result in smaller values of decay rate because the population at the ground state is larger (the ground state is wider). When $w > 0$ the situation turns to the opposite: a narrow ground state squeezes out the particles from it. These features were discussed in ref. [22]. The resulting Kramers rate and the QDR are displayed in figure 6. We see ideal agreement between $R_{\rm K}$ and $R_{\rm D}$. The statistical errors of $R_{\rm D}$ here and in all the relevant figures below are usually about 1% (except Appendix A).

Now we consider the diagonal valleys as in figure 3b when $C_{1c} = C_{1b}$ (i.e. $w = 0$). Here $C_{1c} = C_1(q_{0c})$ when $C_{1b} = C_1(q_{0b})$. Thus, the width of the valley does not depend on q_0 and we vary q_{1b}, i.e. rotate the valley in (q_0, q_1) plane. Results of these calculations are shown in figure 7. We see that $R_{\rm D}$ and $R_{\rm K}$ agree perfectly with each other whereas both of them somewhat decrease as

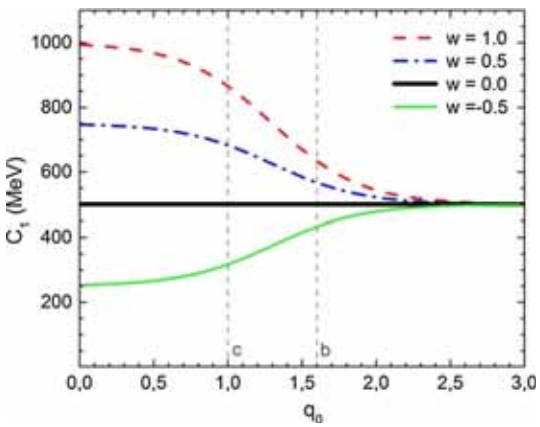

Figure 5. Evolution of the stiffness of the valley with q_0 for several values of w indicated in the figure. The vertical lines correspond to the ground state (c) and to the barrier (b).

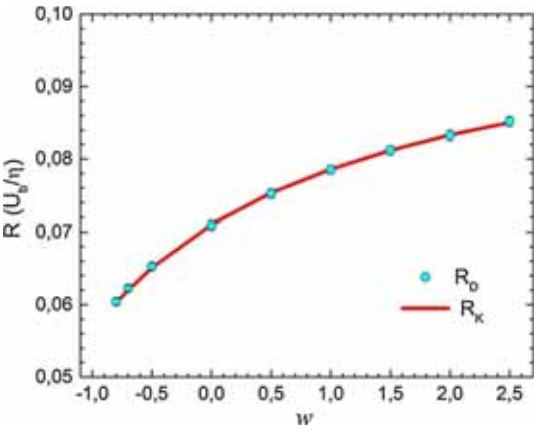

Figure 6. Dependence of the decay rates on the coefficient w in eq. (6). See parameters of the calculations in table B1.

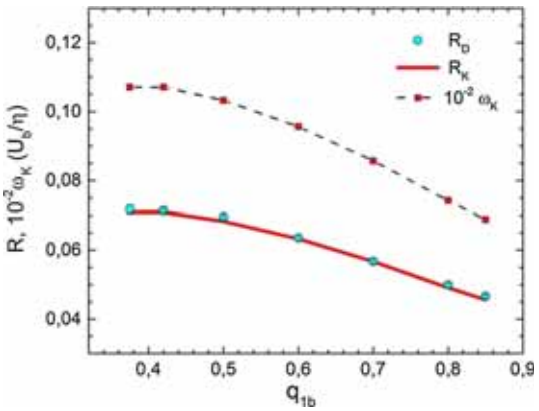

Figure 7. The dependence of the decay rates R_{D}, R_{K} and Kramers frequency ω_{K} on q_{1b}. See parameters of the calculations in table B1.

the valley rotates and the modes couple stronger. Careful analysis of the results shows that this decrease is solely due to the Kramers frequency ω_{K} in eq. (22). This frequency, plotted in figure 7 too, is the least physically clear ingredient of eq. (22). We did not manage to find its physical interpretation in the literature. It looks like ω_{K} is related somehow to the distance between the quasistationary and barrier points: the larger is this distance, the smaller is ω_{K}.

Let us now vary q_{1b} and w simultaneously. The results are presented in table 1 as the fractional difference

$$\xi = R_{\mathrm{K}}/R_{\mathrm{D}} - 1 \tag{24}$$

with the statistical errors (both in percent) for different combinations of C_{1b}/C_{1c} and q_{1b}/q_{1c}. The agreement within the statistical errors not exceeding 1% is observed. Thus, we conclude that the orientation of the valley and the dependence of its stiffness on the elongation coordinate q_0 cannot result in any inaccuracy of the Kramers rate.

3.2 *The influence of the absorptive border*

Let us now see how the Kramers rate measures up against QDR when the absorptive border moves closer to the saddle point being perpendicular to the valley. Here we again consider the case when the valley goes along q_0 coordinate (see figure 3a). Dependence of R_{D} upon q_{0s} (see eq. (7)) at $\phi_{1r} = 0$ is presented in figure 8. The Kramers rate (thick horizontal line) agrees with the QDR (line with symbols) at $q_{0s} > 2.00$ within the statistical errors. As q_{0s} decreases, the QDR exceeds R_{K} and at $q_{0s} \approx q_{0b}$ the R_{D} approaches $2R_{\mathrm{K}}$ (thin horizontal line). This effect was discussed earlier for the 1D case (see, e.g. [13,15]). The physical reason is that those particles which overcome the barrier still have a chance to be returned back into the potential well due to fluctuations if they are not absorbed at the border. In the formula for the Kramers rate, the border is supposed to be very far from the barrier and all these re-scatterings are accounted for. As we move the absorptive border closer to the ridge, some particles of the previously re-scattered ones are absorbed and contribute to the QDR. It was shown in [13,15] that for the 1D case the Kramers rate was to be corrected to account for this effect and the correction factor reached 2 when $q_{0s} \approx q_{0b}$. Thus, the dependence of $R_{\mathrm{D}}/R_{\mathrm{K}}$ as the function of q_{0s} is well understood.

Table 1. The fractional difference between R_{D} and R_{K}, ξ (see eq. (24)), and its absolute statistical error $\Delta\xi$ (in brackets) for different combinations of C_{1b}/C_{1c} and q_{1b}/q_{1c} in the form $\xi(\Delta\xi)$. Both ξ and $\Delta\xi$ are presented in percent; $\Delta\xi = \varepsilon_{\mathrm{R}}$ (see eq. (A2)).

	q_{1b}/q_{1c}				
C_{1b}/C_{1c}	1.00	1.20	1.47	1.73	2.00
0.82	0.12 (0.78)	0.40 (0.78)	0.65 (0.57)	−0.59 (1.00)	−1.16 (0.98)
0.89	0.16 (0.88)	0.64 (0.84)	0.40 (0.72)	0.58 (0.99)	−0.36 (0.74)
1.00	0.16 (0.97)	0.73 (0.69)	0.89 (0.73)	0.65 (1.00)	1.03 (0.76)
1.19	−0.14 (0.82)	0.68 (0.64)	0.39 (0.54)	0.55 (0.82)	0.26 (0.93)
1.35	−0.49 (0.50)	−0.05 (0.85)	−0.02 (0.92)	0.11 (0.77)	−0.48 (0.60)

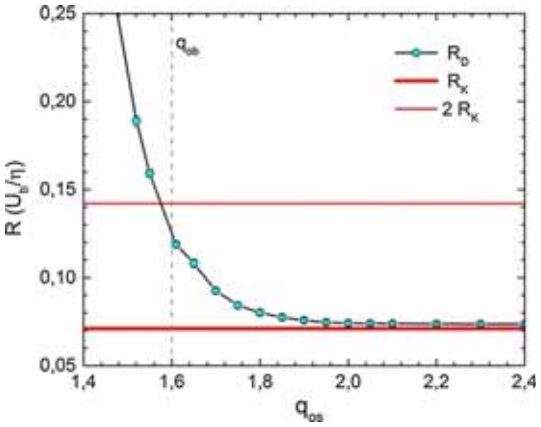

Figure 8. The dependence of the decay rates on q_{0s} for the perpendicular valley. See parameters of the calculations in table B1.

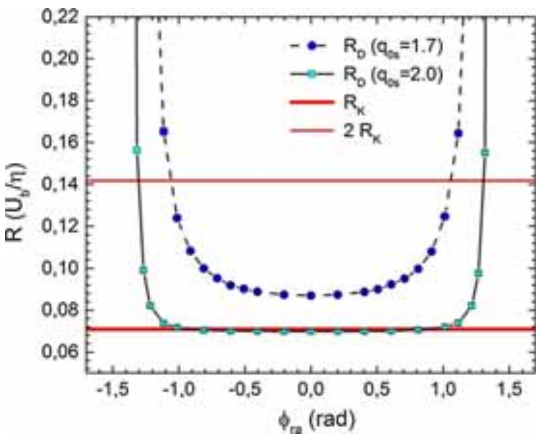

Figure 9. The dependence of the decay rates on the angle between the absorptive border and the ridge, ϕ_{ra}, for the perpendicular valley for two values of q_{0s} indicated in the figure. Other notations are as in the previous figure. See parameters of the calculations in table B1.

As the next step, we study the effect of the slope of the absorptive border at two fixed values of q_{0s}. One of them ($q_{0s} = 2.0$) is large enough, i.e. it corresponds to that part of figure 8 where sensitivity of R_{D} to q_{0s} is absent. The second value ($q_{0s} = 1.7$) is relatively close to the barrier. Results of such calculations are shown in figure 9. The angle between the ridge (perpendicular to the valley) and the absorptive border, ϕ_{ra}, is used here as an argument. We rotate the absorptive border around the point with coordinates q_{0s}, q_{1s} belonging to the valley (see eq. (3)). For symmetry reason, the dependence $R_{\mathrm{D}}(\phi_{ra})$ should be even. One sees in figure 9 that this is the case indeed. Qualitatively we understand the increase of R_{D} with $|\phi_{ra}|$ as follows. Due to the rotation of the absorptive border (line) one half of it is getting further from the ridge. This part of the line does not influence the QDR (see that part of figure 8 for which $q_{0s} > 2$). The other half of the line approaches the ridge and absorbs the particles which otherwise can be re-scattered. The net effect is the increase of R_{D} with the increase of the slope. The following fast increase of R_{D} as $|\phi_{ra}| => \pi/2$ happens because the absorptive border enters the vicinity of the ground state.

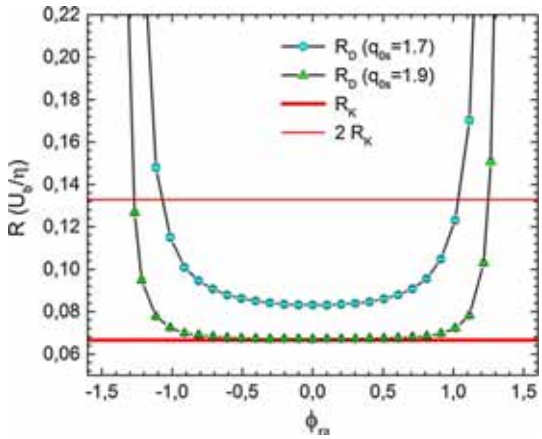

Figure 10. The same as in figure 9 but for the diagonal valley and with the increasing stiffness ($w = -0.2$). See parameters of the calculations in table B1.

Finally, let us consider a general situation in which the diagonal potential is as in figures 2 and 3b and the stiffness is variable with $w = -0.2$ (see eq. (6)). As in figure 9, we rotate the absorptive border around a point in the valley. The minimum value of R_{D} in these calculations is expected when this border is parallel to the ridge. The results are displayed in figure 10, for two cases: $q_{0s} = 1.7$ and 1.9. The dependences $R_{\mathrm{D}}(\phi_{ra})$ look similar to those of figure 9. However, the graphs in figure 10 are somewhat asymmetric with respect to $\phi_{ra} = 0$. The increase of R_{D} at the values of $|\phi_{ra}|$ departing from 0 is explained exactly the same way as in figure 9. The q_0-dependence of C_1 seems to not influence significantly the deviation of R_{K} from R_{D}.

3.3 *The influence of the friction strength*

In order to make our study more comprehensive, we perform calculations for different values of k_η (see eq. (18)). Note that the Kramers rate R_{K} is not valid when friction is so weak that the energy dissipation in one bouncing can be neglected. In the original Kramers work [11] for the latter case, the following formula was obtained:

$$R_{\mathrm{K1}} = \frac{\eta U_b}{mT} \exp\left(-\frac{U_b}{T}\right). \tag{25}$$

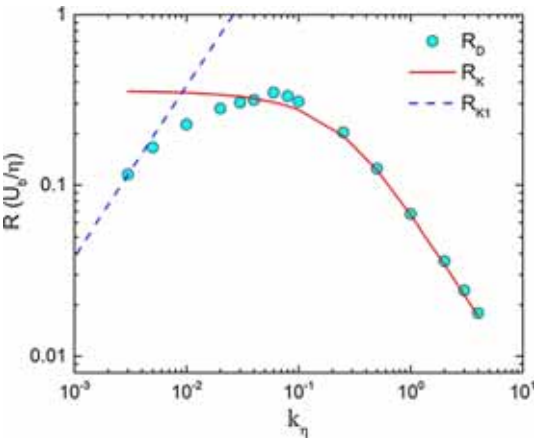

Figure 11. The dependence of the decay rates on the strength of friction k_η (see eq. (18)). Straight dash line indicates the 1D Kramers formula (25), and other notations are as in figures 8, 9, 10. See parameters of the calculations in table B1.

This formula was derived for the 1D motion and we are not aware about its multidimensional generalization. Therefore, we compare in figure 11 the results of numerical modelling with R_{K1} and R_K. Results of this comparison tell us that R_K, in its domain of applicability, is valid for different values of friction strength. Equation (25) also does not contradict the numerical decay rate for ballistic regime (left part of figure 11). We do not manage to obtain the values of R_D for smaller k_η because the Euler–Maruyama algorithm seems to break down.

4. Conclusions

We have studied the accuracy of the Kramers approximate formula (22) for the thermal decay rate of the metastable state for the two-dimensional potential pocket. For this, we have modelled the decay process solving numerically the Langevin-type stochastic equations and building the quasistationary rate on the basis of this solution. The modelling has been performed both for the coupled and uncoupled modes. The potential has been composed of second-order parabolas and thus the anharmonic effects have been excluded.

It has been shown that the Kramers rate is in agreement with the quasistationary rate within the statistical errors (1%) provided the absorptive border is far enough from the potential ridge restricting the metastable state. This result holds for different orientations and shapes of the valley leading from the metastable state. As the absorptive border (or its part) gets closer to the ridge, the Kramers formula underestimates the numerical quasistationary rate. The difference reaches approximately the factor of 2 when the absorptive border coincides with the ridge. These results were obtained earlier for the 1D overdamped case. Thus, it turns out that the influence of the absorptive border on the accuracy of the Kramers formula does not depend on the dimensionality of the modelling and on the strength of friction in the diffusive regime.

Note that according to [15,17] our results can be alternated by the anharmonicity of the potential. The non-diagonal terms of the inertia and friction tensors (as well as the typical for the fission problem coordinate dependence of those tensors) could influence the agreement between the QDR and the Weidenmüller's formula for R_K as well. We plan to address this problem in the near future.

Acknowledgements

MVC is grateful to the Dmitry Zimin Foundation 'Dynasty' for financial support.

Appendix A

Numerical modelling of the random motion of a Brownian particle is based on a pseudorandom number generator. Results of this modelling is a sequence of N_{tot} trajectories, each terminated not later than at t_D. The trajectories which have reached the absorptive border during this time lapse contribute to the decay rate R_{at} calculating according to eq. (21) (see also figure 4). The time dependence of R_{at} can be separated into a nonlinear transition part and a quasistationary part although significant fluctuations may be present. We are interested in the quasistationary value of the rate, R_D, which is calculated as an average value of R_{at} over the quasistationary part

$$R_D = \frac{1}{k}\sum_{j=L-k+1}^{L} R_{at}(t_j). \tag{A1}$$

Here $L = t_D/\Delta t$ is the total number of bins, Δt is the bin width, k is the number of bins used for finding R_D. The initial $(L-k)$ bins are disregarded. The aim of this Appendix is to show that the value of R_D does not depend (within the statistical errors) on Δt, k, and N_{tot}. The statistical error of R_D reads as

$$\varepsilon_R = \frac{1}{R_D\sqrt{k}}\sqrt{\frac{1}{k-1}\sum_{j=L-k+1}^{L}(R_{at}(t_j)-R_D)^2}. \tag{A2}$$

It must decrease as $\sqrt{k}$.

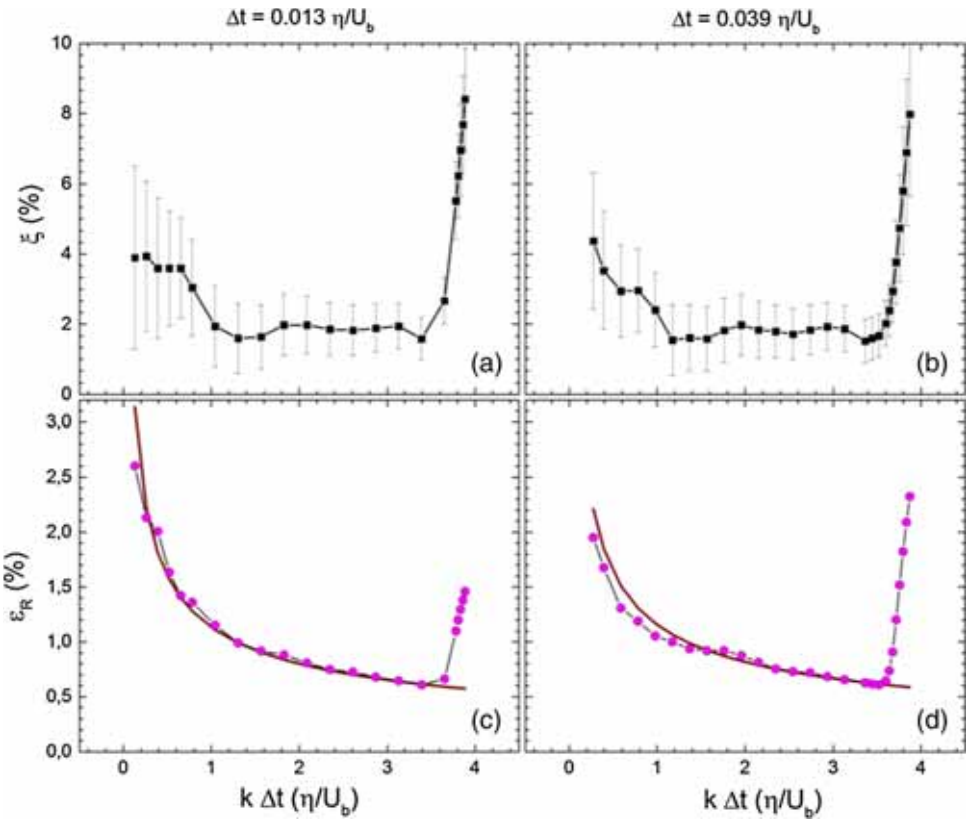

Figure A1. The fractional difference ξ defined by eq. (24) (panels **a** and **b**) and its error ε_R (panels **c** and **d**) vs. the interval of time-averaging $(k\Delta t)$ for two values of Δt (left and right columns). The curves without symbols in panels **c** and **d** represent the $(k\Delta t)^{-1/2}$ dependence and has been adjusted to ε_R at some intermediate points. See parameters of the calculations in table B1.

Table B1. Parameters of modelling for the figures involving decay rate.

Figure	τ, zs	w	q_{1b}	q_{0s}	ϕ_{1r}	ϕ_{ra}	k_η
Figure 4	0.10	0.0	0.700	2.20	0.0	0.0	1
Figure 6	0.05–0.20	Variable	0.375	2.50	0.0	0.0	1
Figure 7	0.10	0.0	Variable	2.00	0.0	0.0	1
Figure 8	0.10	0.0	0.375	Variable	0.0	0.0	1
Figure 9	0.10	0.0	0.375	2.00 and 1.70	0.0	Variable	1
Figure 10	0.10	−0.20	0.500	1.90 and 1.70	0.205	Variable	1
Figure 11	0.01–0.10	−0.20	0.500	1.90	0.205	0.5	Variable
Figures A1, A2	0.10	0.0	0.700	2.20	0.0	0.0	1

$U_b = 6.0\,\text{MeV}$, $\eta = 460\,\text{MeV zs}$, $T = 1.89\,\text{MeV}$, $q_{0b} = 1.6$, $C_{1as} = 500\,\text{MeV}$.

Checking these properties of R_D and ε_R is of importance due to the well-known periodic character of any pseudorandom number generator. The larger is the number of trajectories (and presumably the smaller is ε_R) the larger is the probability of catching this periodicity.

It is convenient to analyse not the QDR itself but its fractional difference from the Kramers rate ξ defined by eq. (24). This fractional difference and its absolute error which is equal to ε_R are shown in figure A1. In the upper panels we see that as the interval of time-averaging $(k\Delta t)$ increases, ξ somewhat decreases and then stays stable, fluctuating within 1%. When $k\Delta t$ exceeds the duration of the quasistationary stage, ξ begins to grow sharply, indicating that R_D gets smaller. This is expected because the transient stage (where R_{at} is significantly smaller than QDR) becomes involved in the calculation. In the lower panels of figure A1 the relative error of R_D, ε_R, is shown. It evolves with $k\Delta t$ according to $k^{-1/2}$ law. As the transient stage starts to be involved, ε_R sharply increases. The curves without symbols in lower panels correspond to $(k\Delta t)^{-1/2}$ dependence and have been adjusted to ε_R at some intermediate points. One

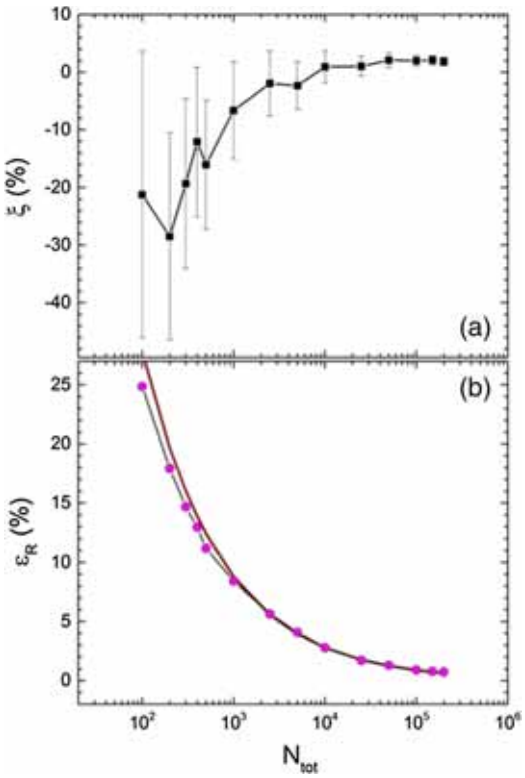

Figure A2. Same as in figure A1 but vs. the total number of trajectories $N_{\rm tot}$. The curve without symbols in panel **b** represents the $N_{\rm tot}^{-1/2}$ dependence and has been adjusted to $\varepsilon_{\rm R}$ at some intermediate points. See parameters of the calculations in table B1.

sees that all these conclusions are unchangeable with respect to the value of Δt (compare the left and right columns).

In figure A2 we present the dependence of $R_{\rm D}$ and $\varepsilon_{\rm R}$ on the number of trajectories. It is seen that as this number increases, $R_{\rm D}$ approaches its constant value and the relative error decreases like $N_{\rm tot}^{-1/2}$ as it is expected. Note that even at very small number of trajectories ($N_{\rm tot} = 100 \div 500$) when the number of useful trajectories reaching the absorptive border is extremely small, our algorithm produces $R_{\rm D}$ which is only 20–30% away from the more correct value corresponding to $2 \cdot 10^5$ trajectories. Therefore, using this algorithm one can obtain a rough estimate of $R_{\rm D}$ very quickly.

Thus, we conclude that all the results of the present paper are valid and no evidence of generator periodicity is seen.

Appendix 2

See table B1.

References

[1] P Hanggi, P Talkner and M Borkovec, *Rev. Mod. Phys.* **62**, 251 (1990)
[2] V I Melnikov, *Phys. Rep.* **209**, 1 (1991)
[3] P Fröbrich and I I Gontchar, *Phys. Rep.* **292**, 131 (1998)
[4] G D Adeev, A V Karpov, P N Nadtochy and D V Vanin, *Phys. Part. Nucl.* **36**, 733 (2005)
[5] Huan-Xiang Zhou, *Quart. Rev. Biophys.* **43(2)**, 219 (2010)
[6] A N Ezin and A L Samgin, *Phys. Rev. E* **82**, 056703 (2010)
[7] R E Lagos and T P Simoes, *Physica A* **390**, 1591 (2011)
[8] Yanjun Zhou and Jiulin Du, *Physica A* **402**, 299 (2014)
[9] K Mazurek, C Schmitt, P N Nadtochy, M Kmiecik, A Maj, P Wasiak and J P Wieleczko, *Phys. Rev. C* **88**, 054614 (2013)
[10] Y Aritomo, S Chiba and F Ivanyuk, *Phys. Rev. C* **90**, 054609 (2014)
[11] H A Kramers, *Physica* **7**, 284 (1940)
[12] O Edholm and O Leimar, *Physica A* **98**, 313 (1979)
[13] I I Gontchar, P Fröbrich and N I Pischasov, *Phys. Rev. C* **47**, 2228 (1993)
[14] I I Gontchar and P Fröbrich, *Nucl. Phys. A* **551**, 495 (1993)
[15] E G Pavlova, N E Aktaev and I I Gontchar, *Physica A* **23**, 6084 (2012)
[16] I I Gontchar and G I Kosenko, *Sov. J. Nucl. Phys.* **53**, 86 (1991)
[17] I I Gontchar, M V Chushnyakova, N E Aktaev, A L Litnevsky and E G Pavlova, *Phys. Rev. C* **82**, 064606 (2010)
[18] E G Demina and I I Gontchar, *Phys. At. Nucl.* **78**, 185 (2015)
[19] L A Pontryagin, A Andronov and A Vitt, *Zh. Eksp. Teor. Fiz.* **3**, 165 (1933) translated by J B Barbour and reproduced in *Noise in nonlinear dynamics* edited by F Moss and P V E McClintock (Cambridge University Press, Cambridge, 1989) Vol. 1, p. 329
[20] G Klein, *Proc. R. Soc. London A* **211**, 431 (1952)
[21] Zhang Jing-Shang and H A Weidenmüller, *Phys. Rev. C* **28**, 2190 (1983)
[22] H A Weidenmüller and Zhang Jing-Shang, *J. Stat. Phys.* **34**, 191 (1984)
[23] I I Gontchar, A E Gettinger, L V Guryan and W Wagner, *Phys. At. Nucl.* **63**, 1688 (2000)
[24] I I Gontchar, *Phys. At. Nucl.* **72**, 1659 (2009)
[25] A V Karpov, P N Nadtochy, E G Ryabov and G D Adeev, *J. Phys. G* **29**, 2365 (2003)
[26] I I Gontchar, N A Ponomarenko, V V Turkin and L A Litnevsky, *Phys. At. Nucl.* **67**, 2080 (2004)
[27] C Schmitt, P N Nadtochy, A Heinz, B Jurado, A Kelic and K-H Schmidt, *Phys. Rev. Lett.* **99**, 042701 (2007)
[28] S G McCalla and J P Lestone, *Phys. Rev. Lett.* **101**, 032702 (2008)
[29] W Ye, *Phys. Rev. C* **81**, 054609 (2010)
[30] M Huang, Z Gan, X Zhou, J Li and W Scheid, *Phys. Rev. C* **82**, 044614 (2010)
[31] K Pomorski and J Dudek, *Phys. Rev. C* **67**, 044316 (2003)
[32] P E Kloeden and E Platen, *Numerical solution of stochastic differential equations* (Springer, Berlin, 1992).
[33] I I Gontchar and S N Krokhin, *Herald of Omsk University* **4**, 84 (2012)
[34] S Hassani and P Grange, *Phys. Lett. B* **137**, 281 (1984)
[35] I I Gontchar and N E Aktaev, *Phys. Rev. C* **80**, 044601 (2009)